Available online at www.sciencedirect.com
ScienceDirect
Trans. Nonferrous Met. Soc. China 25(2015) 2065−2072
Transactions of Nonferrous Metals Society of China
www.tnmsc.cn

Reaction behaviour of Al_2O_3 and SiO_2 in high alumina coal fly ash during alkali hydrothermal process

Zhou-qing JIANG[1,2], Jing YANG[1], Hong-wen MA[1], Le WANG[1,2], Xi MA[1,2]

1. School of Materials Science and Technology, China University of Geosciences, Beijing 100083, China;
2. Blue Sky Technology Corporation, Beijing 100083, China

Received 27 July 2014; accepted 20 January 2015

Abstract: The reaction behaviours of Al_2O_3 and SiO_2 in high alumina coal fly ash under various alkali hydrothermal conditions were studied. The means of XRD, XRF, FTIR and SEM were used to measure the mineral phase and morphology of the solid samples obtained by different alkali hydrothermal treatments as well as the leaching ratio of SiO_2 to Al_2O_3 in alkali solution. The results showed that with the increase of the hydrothermal treating temperature from 75 to 160 °C, phillipsite-Na, zeolite A, zeolite P, and hydroxysodalite were produced sequentially while the mullite and corundum phase still remained. Zeolite P was massively formed at low-alkali concentration and the hydroxysodalite was predominantly obtained at high-alkali concentration. By the dissolution of aluminosilicate glass and the formation of zeolites together, the leaching efficiency of SiO_2 can reach 42.13% with the mass ratio of Al_2O_3/SiO_2 up to 2.19:1.

Key words: high alumina coal fly ash; Al_2O_3; SiO_2; alkali hydrothermal treatment; reaction behaviour

1 Introduction

Coal fly ash (CFA) is the unburned residue after the high temperature combustion of coal and its associated minerals in coal-fired power plant. At present, more than 2.5 billion tons of CFA has been disposed in controlled landfills or waste containment facilities in China [1]. Moreover, with increasing demand for electric power, the ash emission load increased gradually and more than 4 hundred million tons of CFA is discharged every year [2]. Due to the low utilization rate, the CFA has occupied a vast amount of land and posed the serious threat to the environment [3,4]. In recent years, it has been discovered that the coal resources distributing in northern Shanxi and western part of Inner Mongolia China contain high-alumina minerals. The kaolinite and boehmite as the main composition account for 71% and 21% of the total minerals in the coal respectively [5]. The alumina content in CFA generated from this area can reach more than 50%, and the high alumina CFA made it become a potential substituted resource of bauxite for alumina industry [6,7]. Therefore, extraction of alumina from high-alumina CFA not only could solve the problem of bauxite shortage but also avoid the land occupancy and eliminate the environmental pollution.

For the purpose of extracting alumina from CFA efficiently and economically, considerable efforts have been devoted to investigate the different technologies [8,9]. The major methods of recovering alumina from high-alumina CFA can be classified into the mineral acid leaching [10,11], acid−alkali combination [12−14], alkali hydrothermal process [15], lime sintering [16], and desilicated lime−soda sintering processes [17]. The desilicated lime−soda sintering method as an industrializing technology in China to extract alumina from high-alumina CFA [18] included two major steps. The silica extraction step was carried out first using NaOH solution in order to increase the Al_2O_3/SiO_2 mass ratio of the solid; and then the desilicated residue was mixed with lime and sodium carbonate before sintering at 1200 °C, the final alumina extraction efficiency can be up to 90% [17]. Many researchers [19−21] have reported the phase transformation and dissolution mechanism of silica extraction in NaOH solution, but the detailed reaction behaviours of Al_2O_3 and SiO_2 during hydrothermal process have not been clarified adequately. Therefore, it is important to make the behaviours of

Foundation item: Project (2652014017) supported by the Fundamental Research Funds for the Central Universities, China
Corresponding author: Jing YANG; Tel: +86-10-82320512; E-mail: yjcl@cugb.edu.cn
DOI: 10.1016/S1003-6326(15)63816-X

Al_2O_3 and SiO_2 clear in different reaction conditions for the purpose of designing suitable technological process and improving the dissolution efficiency of alumina.

In this work, the reaction behaviours of Al_2O_3 and SiO_2 from high alumina CFA in alkali solution were studied. The research is focused on the effects of the alkali concentration, reaction temperature and leaching time on the crystal structure and morphology of the solid samples formed after alkali-hydrothermal treating CFA as well as the dissolved amount of SiO_2 and Al_2O_3 in alkali solution. The mechanisms of silica leaching during alkali dissolution process were discussed.

2 Experimental

2.1 Materials and instruments

The CFA raw material (GF-12) used in this study was from Zhungeer Power Plant of Guohua Electric Power Corporation, Inner Mongolia, China. The chemical composition of the CFA was analyzed by X-ray fluorescence and the results are listed in Table 1. The high alumina CFA contained 50.71% Al_2O_3 and 40.01% SiO_2 with an Al_2O_3/SiO_2 mass ratio of 1.25:1. The contents of major phase were crystalline mullite and corundum as well as amorphous aluminosilicate glass phase. The sodium hydroxide used in the experiments was of analytical grade from Beijing Chemical Factory, China.

Table 1 Chemical composition of CFA used in experiments (mass fraction, %)

SiO_2	TiO_2	Al_2O_3	Fe_2O_3	MgO	CaO	LOI
40.01	1.57	50.71	1.80	0.47	2.85	1.41

Thermostatic oil-bath (HH-SH2) was made in Meite Instrument Company, China, which consisted of an oil bath and a magnetic stirring system. The silicone oil was used as the fluid-heating medium. The sealed reaction container of 100 mL was prepared from Teflon to avoid corrosion under different temperature and alkali liquor condition.

2.2 Experimental process and analytical methods

The high-alumina CFA (10 g) was mixed with 1.0−10.0 mol/L NaOH solution in a 100 mL Teflon vessel and using appropriate solid to liquid ratio of 1 g/4 mL. The mixture was heated in thermostatic oil-bath under magnetic stirring. The oil bath temperature was set from 75 to 160 °C and the treating time changed from 0.5 to 10 h in order to investigate the reaction behaviours of the Al_2O_3 and SiO_2 at different alkali hydrothermal processes. The mixture solution after hydrothermal treatment was filtered and washed with 75 °C deionized water, and then the solid residue was dried at 105 °C for 24 h.

X-ray diffraction (XRD) powder analysis was recorded using a SmartLab (Rigaku) X-ray diffractometer in step of 0.02° using Cu K_α radiation and a scanning speed of 8.0 (°)/min. The morphology of the CFA and the prepared solid samples were examined via Sirion 200 scanning electron microscopy (SEM) under the analytical conditions of EHT=5.00 kV and signal A=SE. FT-IR spectra were collected using Perkin Elmer 2000 in the 4000−400 cm^{-1} region using potassium bromide as the diluent and binder. The contents of alumina and silica were tested using the Supermini (Rigaku) X-ray fluorescence (XRF) analyzer. The alkali dissolution leaching efficiency was obtained by the following formulas:

$$\eta(Al_2O_3)=\frac{m_{CAF}(Al_2O_3)-m_{RE}(Al_2O_3)}{m_{CAF}(Al_2O_3)}\times 100\% \quad (1)$$

$$\eta(SiO_2)=\frac{m_{CAF}(SiO_2)-m_{RE}(SiO_2)}{m_{CAF}(SiO_2)}\times 100\% \quad (2)$$

where η is the leaching efficiency; $m_{CAF}(Al_2O_3)$ and $m_{RE}(Al_2O_3)$ donate the mass of Al_2O_3 in the CFA and filtrate, $m_{CAF}(SiO_2)$ and $m_{RE}(SiO_2)$ donate the mass of SiO_2 in the CFA and filtrate respectively.

3 Results and discussion

3.1 Effect of alkalinity

The XRD patterns of the CFA and products obtained in hydrothermal reaction with various NaOH concentrations at 95 °C for 4 h are shown in Fig. 1. It can be seen that the main crystalline compounds of raw CFA were mullite ($3Al_2O_3{\cdot}2SiO_2$) and corundum (α-Al_2O_3), which were typical low-CaO and high-Al_2O_3 CFA. This further indicated a pronounced broad hump in the background approximately 22° (2θ), which resulted from

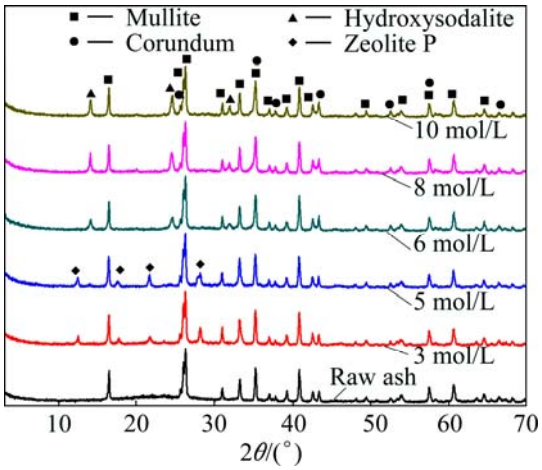

Fig. 1 XRD patterns of raw CFA and products obtained in NaOH solutions with different concentrations

the diffuse scattering of the X-ray due to the presence of amorphous phase. After the hydrothermal treatment, the diffuse scattering disappeared while zeolite P ($Na_{3.6}Al_{3.6}Si_{12.4}O_{32}·14H_2O$) was formed and its crystal diffraction peaks intensity increased with an increase of NaOH concentration below 5 mol/L. When the alkali concentration was added to 6 mol/L, the zeolite P disappeared along with the formation of hydroxysodalite [$Na_8Al_6Si_6O_{24}(OH)_2·(H_2O)_2$]. The diffraction intensity of hydroxysodalite increased above 6 mol/L concentration while the diffraction intensities of mullite and corundum crystal remain unchanged. MURAYAMA et al [22] reported that the zeolite crystals changing from zeolite P to hydroxysodalite did not happen by the hydrothermal reaction, and they deposited at the beginning of crystallization process as the initial crystals.

The reaction behaviours of the CFA in alkali solution with different concentrations were further investigated by SEM. Surface structures of the products obtained in NaOH solutions with different concentrations are presented in Fig. 2. The raw CFA particles were spherical in shape and exhibited a relatively smooth surface texture (Fig. 2(a)). This particle contained an exterior aluminosilicate glass hull with some small grain deposits followed by a near surface layer of mullite and corundum crystalline phase and an interior glass matrix. After hydrothermal reaction in 3 mol/L NaOH solution, the CFA residue morphology (Fig. 2(b)) showed that the smooth aluminosilicate glass surface disappeared and strip grain crystal was exposed, meanwhile, a number of new particles formed adhering on the spherical residue surface. Combined with the results of Fig. 1, the facts that the aluminosilicate glass surface was dissolved by alkali solution and zeolite P formed during the reaction were confirmed. When the NaOH concentration was above 6 mol/L, it was clearly observed that the quasi-spherical aggregate particles (Figs. 2(d)−(f)) appeared on the CFA residue surface and the diameter increased from 1 to 4 μm.

The SiO_2 and Al_2O_3 leaching efficiencies and the Al_2O_3/SiO_2 mass ratio in the solid samples after the hydrothermal reaction with different NaOH solutions at

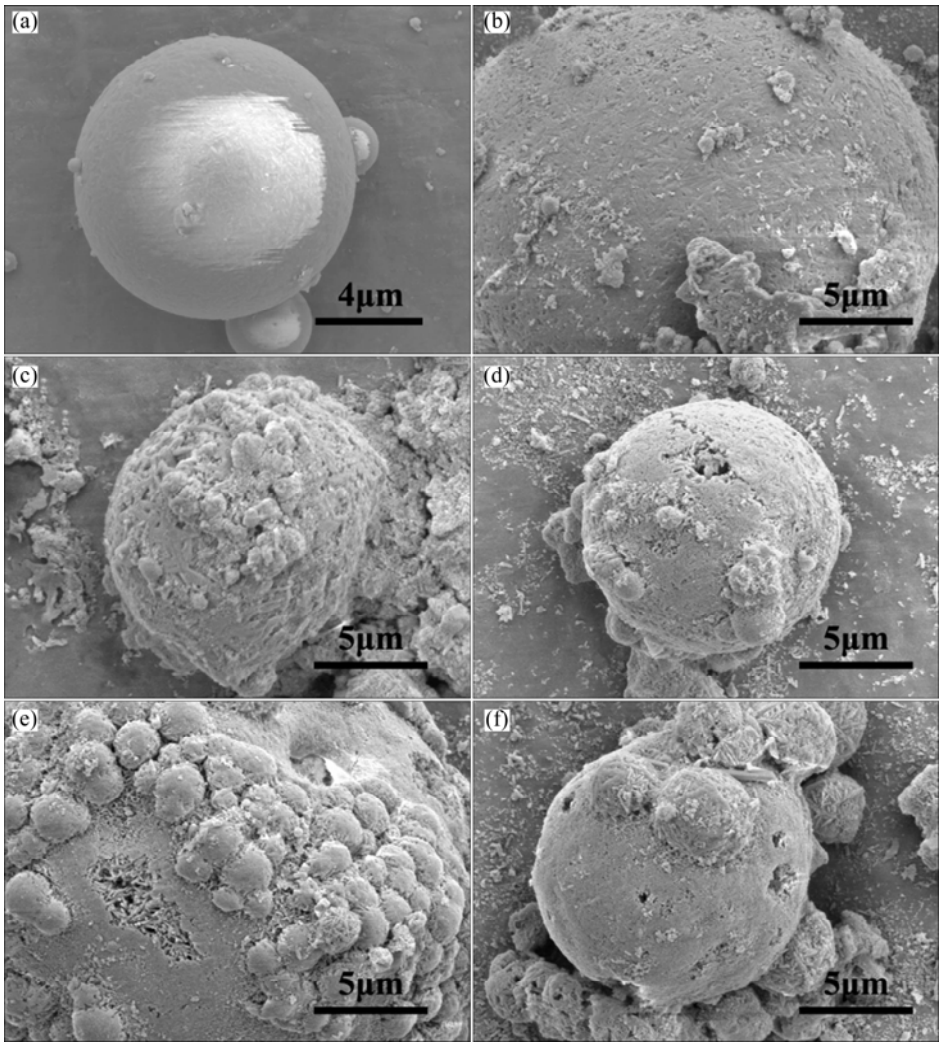

Fig. 2 SEM images of solid samples obtained in NaOH solutions with different concentrations: (a) Raw ash; (b) 3 mol/L; (c) 5 mol/L; (d) 6 mol/L; (e) 8 mol/L; (f) 10 mol/L

95 °C for 4 h are shown in Fig. 3. The SiO_2 leaching efficiency increased with increasing alkali concentration and became constant at about 38.79% at alkali concentration of 6 mol/L. The Al_2O_3 leaching efficiency also increased with alkali concentration below 3 mol/L but decreased before reaching the minimum leaching efficiency of 7.22% at alkali concentration of 6 mol/L, then increased slightly at higher concentrations. Therefore, the Al_2O_3/SiO_2 mass ratio of the solid samples increased with alkali concentration raising firstly and then decreased after reaching the maximum leaching efficiency of 2.08% at alkali concentration of 6 mol/L.

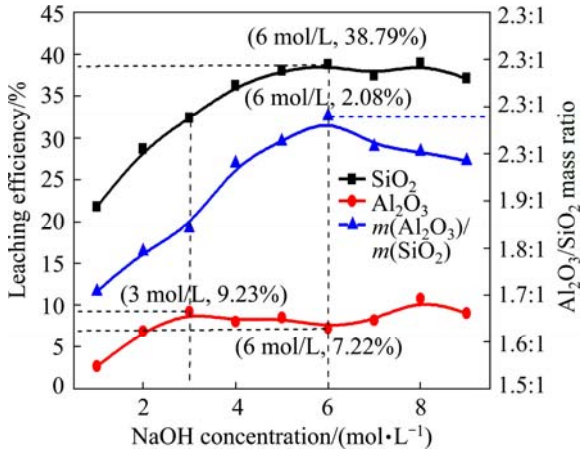

Fig. 3 SiO_2 and Al_2O_3 leaching efficiency and Al_2O_3/SiO_2 mass ratio of solid samples obtained in NaOH solutions with different concentrations

The structure of zeolite is made up of framework of $[SiO_4]^{4-}$ and $[AlO_4]^{5-}$ tetrahedral linked to each other at the corners by sharing their oxygens [23]. After alkali-hydrothermal treatment, the aluminosilicate glass phase disappeared and the ingredient of Al_2O_3 and SiO_2 in glass dissolved into solution. With the increase of alkali concentration, a range of $[SiO_3]^{2-}$ anions may appear with various degrees of oligomerization while $[Al(OH)_4]^-$ is always the dominant anion form of alumina [24]. In alkali solution, the $[SiO_3]^{2-}$ oligomerization combined with $[Al(OH)_4]^-$ to turn into zeolites whose composition and ranges of kinetic stability depend on the alkalinity of the solution [25]. In this experiment, using high alumina CFA as raw material, the hydroxysodalite was obtained at high alkali concentration and the zeolite P was synthesized at low concentration, and these results were similar to those of the previous research [26]. In addition, an increase in OH^- concentration would generally lead to an accelerated crystal growth and shortened nuclei formed time, so the diameter of the hydroxysodalite aggregate particles increased gradually with the increase of NaOH concentrations. When the final products transformed from zeolite P ($Na_{3.6}Al_{3.6}Si_{12.4}O_{32}·14H_2O$) to hydroxysodalite at alkali concentration of 6 mol/L, the Al/Si molar ratio in zeolite was improved from 1:3.4 to 1:1 which also led to more soluble $[Al(OH)_4]^-$ precipitating and the Al_2O_3/SiO_2 mass ratio improving in the solid samples. The fact that the Al_2O_3 leaching efficiency increased at higher alkali concentration seemed to be caused by the small amount of crystalline mullite dissolved in the reaction at such a high-NaOH concentration.

3.2 Effect of hydrothermal treating temperature

The XRD patterns of the solid samples obtained in 4 mol/L NaOH solution for 4 h are shown in Fig. 4 as a function of hydrothermal-treating temperature. As can be clearly seen, some kinds of zeolites were acquired at different hydrothermal-treating temperatures. At 75 °C, a little phillipsite−Na ($Na_{6.4}Al_{6.4}Si_{9.6}O_{32}·4.6H_2O$) was formed, while the diffuse scattering of the X-ray at 22° (2θ) still existed, indicating that the aluminosilicate glass of CFA was not dissolved completely. When the hydrothermal temperature increased to 85 °C, the phillipsite−Na was gradually reduced accompanied with a new phase of zeolite P appearing, and the aluminosilicate glass disappeared in the prepared solids. When the temperature was up to 120 °C, zeolite P, zeolite A ($Na_{96}Al_{96}Si_{96}O_{384}·14H_2O$) and hydroxysodalite were obtained simultaneously. It was reported that higher temperatures led to the crystallization of more dense products [22]. In this study, zeolite P and zeolite A disappeared when the hydrothermal temperature reached 160 °C but the diffraction intensity of hydroxysodalite increased under this condition. On the other hand, the diffraction intensities of mullite and corundum, which are the stable crystalline substance in CFA, did not change during the hydrothermal reaction until temperature reached 160 °C, which were agreed with the previous research results [19].

Figure 5 implies the SEM images of the products

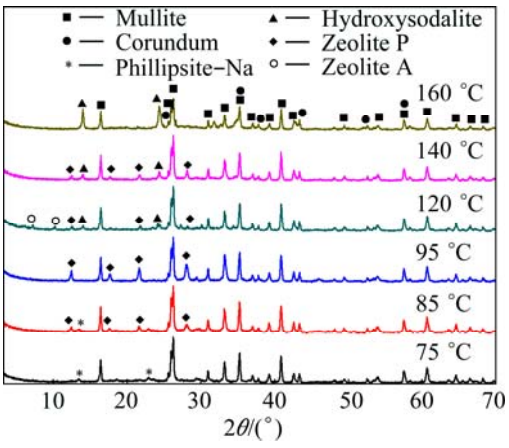

Fig. 4 XRD patterns of products obtained at different treating temperatures

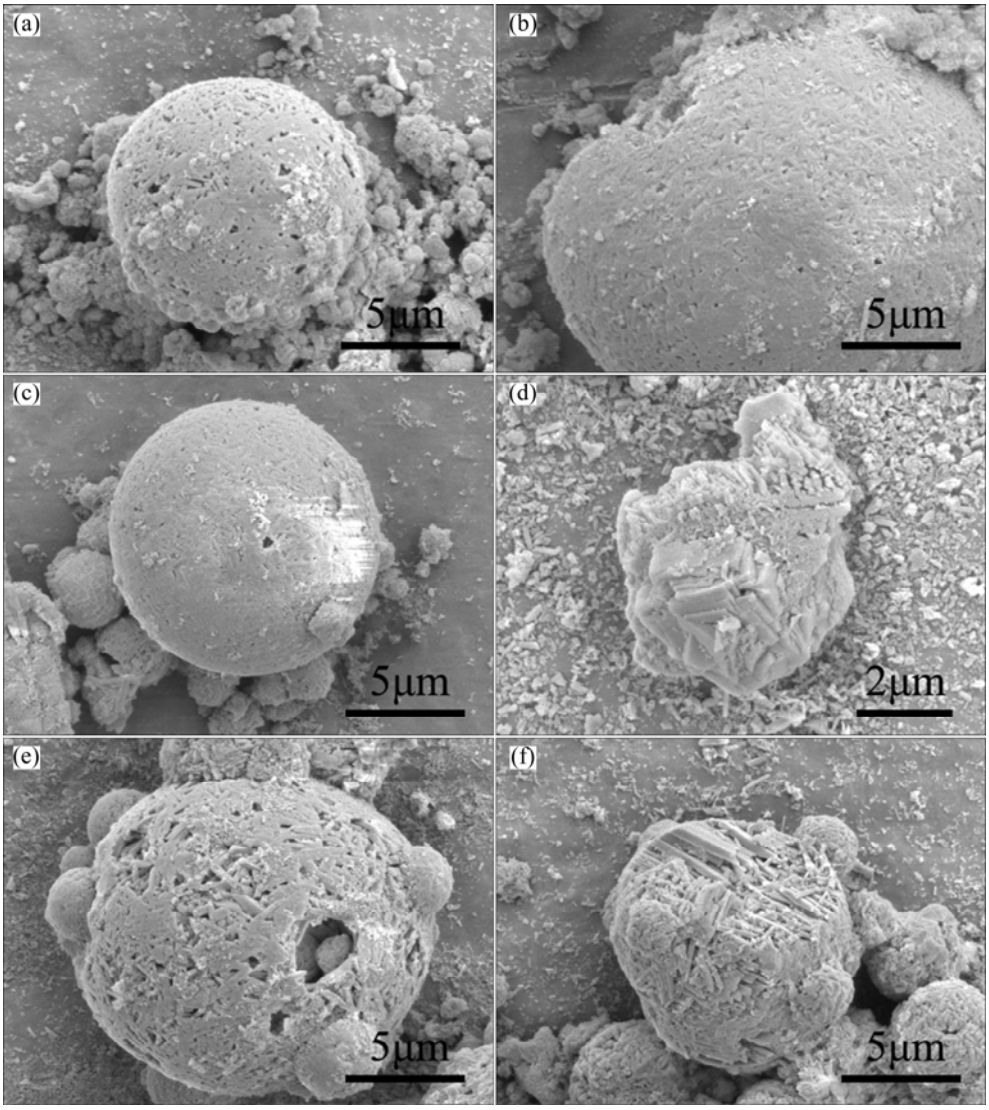

Fig. 5 SEM images of products obtained at different treating temperatures: (a) 75 °C; (b) 85 °C; (c) 95 °C; (d) 120 °C; (e) 140 °C; (f) 160 °C

obtained in 4 mol/L NaOH solution for 4 h at different treating temperatures. The amorphous aluminosilicate hulls in CFA were dissolved partly and the crystalline mullite exposed on the surface of spherical CAF particles when the temperature was 75 °C (Fig. 5(a)). Corresponding to the phenomena of zeolites produced in Fig. 4, the small particles changed their morphology with the temperature increasing, and the quasi-spherical aggregate particles with the diameter of 2−5 μm formed at 160 °C. Moreover, the high temperatures increased the ability of alkali corrosion and the strip mullite crystal particles inside the spherical CFA were partly dissolved, showing the inner texture of particle (Fig. 5(f)).

The SiO_2 and Al_2O_3 leaching efficiencies and the Al_2O_3/SiO_2 mass ratio in the solid samples after the hydrothermal reaction in 4 mol/L NaOH solution at different temperatures for 4 h are shown in Fig. 6. It was seen that the leaching efficiencies of Al_2O_3 and SiO_2 in

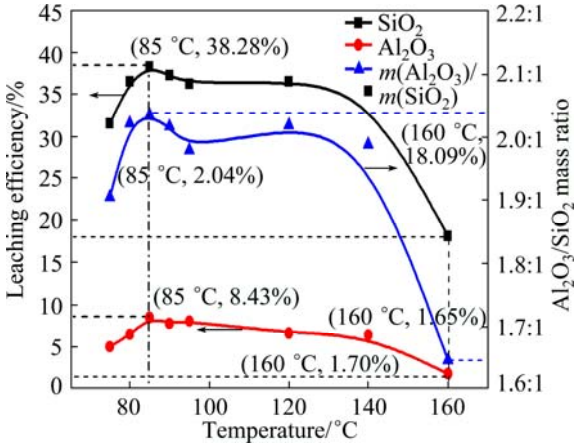

Fig. 6 SiO_2 and Al_2O_3 leaching efficiencies and Al_2O_3/SiO_2 mass ratio of solid samples obtained at different temperatures

the CFA significantly increased instantaneously when the temperature was below 85 °C and reached the maximum

efficiencies of 38.28% and 8.43%, respectively. With the reaction temperature rising, the SiO_2 and Al_2O_3 ingredient leaching efficiencies presented the tendency of decreasing which meant that more SiO_2 remained in the solid. Especially, when the hydrothermal temperature was up to 160 °C, both SiO_2 and Al_2O_3 leaching efficiencies reduced sharply while the Al_2O_3/SiO_2 mass ratio decreased as well. Combining with the results of Figs. 4 and 5, it was suggested that the extraction efficiencies of SiO_2 and Al_2O_3 were controlled by the dissolution of aluminosilicate glass and the formation of zeolites together. At lower hydrothermal temperatures, the speed of zeolite formation was slow and the amount of soluble $[SiO_3]^{2-}$ and $[Al(OH)_4]^-$ increased with the dissolution of glass phase. High temperatures would accelerate the crystallization of zeolite, which led to the decrease of soluble $[SiO_3]^{2-}$ and $[Al(OH)_4]^-$ ions concentration and then reached equilibrium in alkali solution. When the reaction temperature was increased to 160 °C, more aluminate ions were supplied because of the mullite crystal dissolution in CFA, and the mass of soluble $[SiO_3]^{2-}$ and $[Al(OH)_4]^-$ was precipitated and formed hydroxysodalite with a Al/Si molar ratio of 1:1. As a result, the leaching efficiencies of SiO_2 and Al_2O_3 as well as the Al_2O_3/SiO_2 mass ratio in CFA residue decreased significantly.

3.3 Effect of treating time

Figure 7 shows the XRD patterns of the products obtained in different reaction time with 6 mol/L NaOH solution at 95 °C. After a treatment in alkali solution for 2 h, the hydroxysodalite phase appeared. With the prolonging of treating time to 10 h, the XRD peak intensity of hydroxysodalite increased gradually while other new phases were not detected in solid samples. SiO_2 and Al_2O_3 leaching efficiencies and the Al_2O_3/SiO_2 mass ratio in CFA reaction residue during the hydrothermal reaction for different time are shown in Fig. 8. From the results, the SiO_2 extraction efficiency increased at early state and peaked to 42.13% after 2 h. For reaction time over 5 h, the leaching efficiency of SiO_2 reduced to 38.04% and then remained largely unchanged. On the other hand, the Al_2O_3 leaching efficiency increased to 8.21% and then remained stable as well. The Al_2O_3/SiO_2 mass ratio in CFA residue was positively related to the SiO_2 leaching ratio and it peaked to 2.19% after 2 h hydrothermal treatment time. The results suggested that 2 h of leaching time was sufficient for improving the Al_2O_3/SiO_2 mass ratio of CFA. In contrast, an extension in leaching time did not seem to increase the dissolved amount of SiO_2.

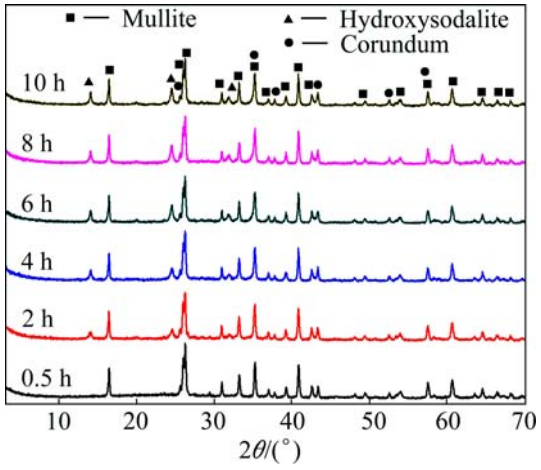

Fig. 7 XRD patterns of products obtained in different treating time

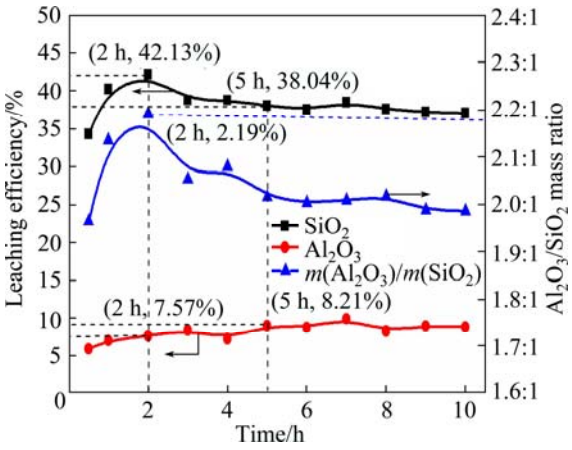

Fig. 8 SiO_2 and Al_2O_3 leaching efficiencies and Al_2O_3/SiO_2 mass ratio of CAF for different reaction time

The hydrothermal-treating time has an important influence on the reaction behaviours of Al_2O_3 and SiO_2 during alkali hydrothermal process. The thermodynamically least favorable phase crystallized first and then was successively replaced in time by more stable phases. The FTIR spectra of CFA and products after the hydrothermal treatment in 6 mol/L NaOH solution at 95 °C for different time are shown in Fig. 9. From the curve of the raw CFA, the vibration of water produced bands at 3450 and 1650 cm^{-1}, the wide band appearing between 1350 and 750 cm^{-1} was due to the vibration of $[SiO_4]^{4-}$ and $[AlO_4]^{5-}$ [27]. The components appearing at about 1078 cm^{-1} and 996 cm^{-1} were attributed to the vitreous phase of raw ash while the presence of mullite was responsible for the characteristic bands at 1145 cm^{-1} and 1185 cm^{-1} [28]. After hydrothermal treatment, the band centering at 1078 cm^{-1} and 996 cm^{-1} disappeared gradually and a new component caused by the OH^- bending vibration appeared at around 1650 cm^{-1}. At the same time, the bands located at 986 cm^{-1} and 729 cm^{-1} which were the asymmetric stretch band and symmetric stretch of hydroxysodalite [29] were clearly detected after hydrothermal reaction for 1 h. The bands at 1145

cm^{-1} and 1185 cm^{-1} still kept unchanged during different reaction time.

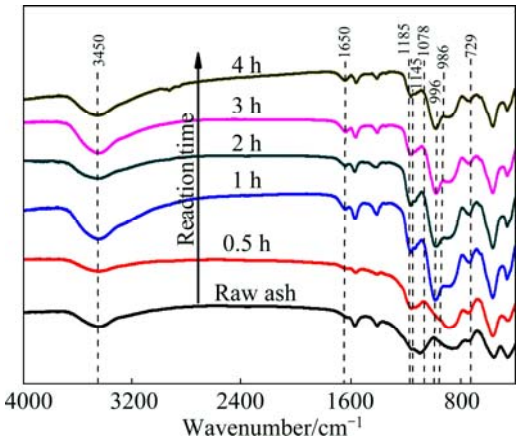

Fig. 9 FTIR spectra of CFA and products after hydrothermal treatment in NaOH solution for different time

In the early reaction period, the amorphous Al_2O_3 and SiO_2 species were dissolved in the form of different oligomerization. Hydrothermal treatment led to the disappearance of glass phase on the fly ash particle surface as well as the raise of aluminate ions and silicate ions in alkali solution. On the other hand, the aluminate ions and silicate ions were precipitated to form aluminosilicate gel which was a precursor of zeolite crystal [22]. As the precipitation reaction proceeds, the aluminosilicate gel rapidly deposited on the spherical particle surface and then transformed to zeolite crystals. The reaction of precipitation and transform made the aluminate ions and silicate ions in solution be consumed until reached an equilibrium state. Leaching ratio was, therefore, dependent on the dissolution of glass phase and the precipitation of zeolite phase.

4 Conclusions

1) The Al_2O_3 and SiO_2 of high alumina CFA presented different reaction behaviours at various alkali hydrothermal conditions. Alkali concentration, hydrothermal temperature and time have significant influence on the mineral phase and morphology of the solid products as well as leaching efficiency of SiO_2 in CFA. After alkali hydrothermal treatment of the CFA, the amorphous Al_2O_3 and SiO_2 dissolved into alkaline solution with the forms of various $[SiO_3]^{2-}$ oligomerization and $[Al(OH)_4]^-$ respectively, and then the silicate ions and aluminate ions were precipitated on the spherical particle surface to form different zeolites through gelation and transformation process. Zeolite P was obtained at lower alkali concentrations while hydroxysodalite formed at higher NaOH concentrations. With the hydrothermal treating temperature increasing, phillipsite−Na, zeolite A, zeolite P, and hydroxysodalite can be obtained sequentially in 4 mol/L alkali solution. The content of mullite and corundum in CFA kept unchanged until the temperature was up to 160 °C.

2) The SiO_2 and Al_2O_3 leaching efficiencies of CFA were dependent on the dissolution of glass phase and the precipitation of zeolite phase. Increasing alkali concentration and temperature was beneficial to the dissolution of glass phase. However, higher temperature and more time would also advance the production of zeolites which decreased the leaching efficiency of SiO_2. When the high alumina CFA was treated at 95 °C for 2 h in 6 mol/L alkali solution, most of the glass phase in the CFA was dissolved and the SiO_2 leaching efficiency reached 42.13% with the Al_2O_3/SiO_2 mass ratio up to 2.19:1.

References

[1] YANG Jing, JIANG Zhou-qing, MA Hong-wen, SU Shuang-qing, WANG Ming-wei, LI Jin-hong, YAO Wen-gui. The bauxite resource in China and advances in the techniques of extracting alumina from high-alumina coal fly ash [J]. Earth Science Frontiers, 2014, 21(5): 313−324. (in Chinese)

[2] LU Guo-yi, XUE Feng, ZHAO Jiang-tao. Some advice to the fly ash of China [J]. China Mining Magazine, 2011, 20: 193−200. (in Chinese)

[3] MARTINELLO K, OLIVEIRA M L, MOLOSSI F A, RAMOS C G, TEIXEIRA E C, KAUTZMANN R M, SILVA L F. Direct identification of hazardous elements in ultra-fine and nanominerals from coal fly ash produced during diesel co-firing [J]. Science of The Total Environment, 2014, 470: 444−452.

[4] IZQUIERDO M, QUEROL X. Leaching behaviour of elements from coal combustion fly ash: An overview [J]. International Journal of Coal Geology, 2012, 94: 54−66.

[5] SHAO Long-yi, CHEN Jiang-feng, SHI Yu-zhen, LU Jing. Minerals in feed coal and their contribution to high-alumina fly ash in the jungar power plant [J]. Journal of China Coal Society, 2007, 32: 411−415. (in Chinese)

[6] QI L Q, YUAN Y T. Characteristics and the behavior in electrostatic precipitators of high-alumina coal fly ash from the Jungar power plant, Inner Mongolia, China [J]. Journal of Hazardous Materials, 2011, 192: 222−225.

[7] FENG C, YAO Y, LI Y, LIU X, SUN H. Thermal activation on calcium silicate slag from high-alumina fly ash: A technical report [J]. Clean Technologies and Environmental Policy, 2014, 16: 667−672.

[8] BLISSETT R, ROWSON N. A review of the multi-component utilisation of coal fly ash [J]. Fuel, 2012, 97: 1−23.

[9] SHEMI A, MPANA R, NDLOVU S, van DYK L, SIBANDA V, SEEPE L. Alternative techniques for extracting alumina from coal fly ash [J]. Minerals Engineering, 2012, 34: 30−37.

[10] WU Cheng-you, YU Hong-fa, ZHANG Hui-fang. Extraction of aluminum by pressure acid-leaching method from coal fly ash [J]. Transactions of Nonferrous Metals Society of China, 2012, 22(9): 2282−2288.

[11] NAYAK N, PANDA C R. Aluminium extraction and leaching characteristics of talcher thermal power station fly ash with sulphuric acid [J]. Fuel, 2010, 89: 53−58.

[12] GUO Y X, LI Y Y, CHENG F Q, WANG M, WANG X M. Role of additives in improved thermal activation of coal fly ash for alumina extraction [J]. Fuel Processing Technology, 2013, 110: 114−121.

[13] BAI G H, QIAO Y H, SHEN B, CHEN S L. Thermal decomposition of coal fly ash by concentrated sulfuric acid and alumina extraction process based on it [J]. Fuel Processing Technology, 2011, 92: 1213−1219.
[14] WANG Ruo-chao, ZHAI Yu-chun, WU Xiao-wei, NING Zhi-qiang, MA Pei-hua. Extraction of alumina from fly ash by ammonium hydrogen sulfate roasting technology [J]. Transactions of Nonferrous Metals Society of China, 2014, 24(5): 1596−1603.
[15] YANG Quan-chen, MA Shu-hua, ZHENG Shi-li, ZHANG Ran. Recovery of alumina from circulating fluidized bed combustion Al-rich fly ash using mild hydrochemical process [J]. Transactions of Nonferrous Metals Society of China, 2014, 24(5): 1187−1195.
[16] MATJIE R, BUNT J, van HEERDEN J. Extraction of alumina from coal fly ash generated from a selected low rank bituminous South African coal [J]. Minerals Engineering, 2005, 18: 299−310.
[17] BAI Guang-hui, TENG Wei, WANG Xiang-gang, QIN Jin-guo, XU Peng, LI Peng-cheng. Alkali desilicated coal fly ash as substitute of bauxite in lime-soda sintering process for aluminum production [J]. Transactions of Nonferrous Metals Society of China, 2010, 20(S): s169−s175.
[18] YAO Z, XIA M, SARKER P, CHEN T. A review of the alumina recovery from coal fly ash, with a focus in China [J]. Fuel, 2014, 120: 74−85.
[19] SU S Q, YANG J, MA H W, JIANG F, LIU Y Q, LI G. Preparation of ultrafine aluminum hydroxide from coal fly ash by alkali dissolution process [J]. Integrated Ferroelectrics, 2011, 128: 155−162.
[20] RATTANASAK U, CHINDAPRASIRT P. Influence of NaOH solution on the synthesis of fly ash geopolymer [J]. Minerals Engineering, 2009, 22: 1073−1078.
[21] LI H Q, HUI J B, WANG C Y, BAO W J, SUN Z H. Extraction of alumina from coal fly ash by mixed-alkaline hydrothermal method [J]. Hydrometallurgy, 2014, 147−148: 183−187.
[22] MURAYAMA N, YAMAMOTO H, SHIBATA J. Mechanism of zeolite synthesis from coal fly ash by alkali hydrothermal reaction [J]. International Journal of Mineral Processing, 2002, 64: 1−17.
[23] QUEROL X, MORENO N, UMANA J T, ALASTUEY A, HERN NDEZ E, L PEZ-SOLER A, PLANA F. Synthesis of zeolites from coal fly ash: An overview [J]. International Journal of Coal Geology, 2002, 50: 413−423.
[24] BYRAPPA K, YOSHIMURA M. Handbook of hydrothermal technology [M] 2nd ed. New York: William Andrew, 2012.
[25] LECHERT H. The pH value and its importance for the crystallization of zeolites [J]. Microporous and Mesoporous Materials, 1998, 22: 519−523.
[26] AHMARUZZAMAN M. A review on the utilization of fly ash [J]. Progress in Energy and Combustion Science, 2010, 36: 327−363.
[27] PENILLA R P, BUSTOS A G, ELIZALDE S G. Zeolite synthesized by alkaline hydrothermal treatment of bottom ash from combustion of municipal solid wastes [J]. Journal of the American Ceramic Society, 2003, 86: 1527−1533.
[28] CRIADO M, FERN NDEZ-JIM NEZ A, PALOMO A. Alkali activation of fly ash: Effect of the SiO_2/Na_2O ratio: Part I: FTIR study [J]. Microporous and Mesoporous Materials, 2007, 106: 180−191.
[29] NOVEMBRE D, DI SABATINO B, GIMENO D, GARCIA-VALL S M, MART NEZ-MANENT S. Synthesis of Na–X zeolites from tripolaceous deposits (Crotone, Italy) and volcanic zeolitised rocks (Vico volcano, Italy) [J]. Microporous and Mesoporous Materials, 2004, 75: 1−11.

高铝粉煤灰中 Al_2O_3 与 SiO_2 在碱溶液中的反应行为

蒋周青[1,2]，杨 静[1]，马鸿文[1]，王 乐[1,2]，马 玺[1,2]

1. 中国地质大学(北京) 材料科学与工程学院，北京 100083；
2. 昊青薪材(北京) 技术有限公司，北京 100083

摘 要：研究高铝粉煤灰中 Al_2O_3 与 SiO_2 组分在 NaOH 碱液中不同水热条件下的反应行为。采用 XRD、XRF、SEM、FTIR 等测试方法对高铝粉煤灰碱溶液处理前后的物相组成和形貌变化进行表征，得到粉煤灰 Al_2O_3 和 SiO_2 组分的溶出率变化规律。结果表明，高铝粉煤灰经 75 °C 到 160 °C 不同温度碱溶液处理后，颗粒表面硅铝玻璃相消失，依次生成钠型沸石、A 型沸石、P 型沸石及羟基方钠石，所含刚玉及莫来石相未被完全溶解。在低碱浓度溶液中 P 型沸石为主要生成相，高碱浓度下羟基方钠石为稳定的相。在铝硅玻璃体溶解和沸石相生成两种反应的共同作用下，粉煤灰中 SiO_2 的溶出率可达 42.13%，滤渣中 Al_2O_3/SiO_2 质量比提高到 2.19:1.

关键词：高铝粉煤灰；Al_2O_3；SiO_2；碱液处理；反应行为

(Edited by Xiang-qun LI)